Journal of Sound and Vibration (1993) **166**(3), 463–476

THE STABILITY AND RESPONSE OF A FLEXIBLE ROD IN A QUICK RETURN MECHANISM: LARGE CRANK CASE

D. G. BEALE

Department of Mechanical Engineering, Auburn University, Auburn, Alabama 36849, *U.S.A.*

AND

R. A. SCOTT

Department of Mechanical Engineering and Applied Mechanics, The University of Michigan, Ann Arbor, Michigan 48109, *U.S.A.*

(*Received* 10 *April* 1991, *and in final form* 16 *April* 1992)

The response and stability of a flexible rod, rigid crank quick return mechanism is investigated without a small crank restriction. A Galerkin's approach was found to be too computationally intensive, due to the moving boundary and complex mode shapes, and thus unsuitable for monodromy based parametric resonance stability investigations. A simple set of polynomial modes were developed. Although requiring more modes than the Galerkin method to obtain the same accuracy, polynomial modes require less computation time for stability investigations. A free–free (time independent) mode method was used to obtain non-linear dynamical and constraint equations. The method was found to be the most accurate and least computationally expensive for response; however, these equations were non-linear and not suitable for stability investigations.

1. INTRODUCTION

The quick return mechanism shown in Figure 1 has several industrial applications. Modelling the crank as a rigid body and the rod as a flexible beam, it was previously treated by the authors [1], under the restriction of a small crank length. That restriction allowed approximations (in the form of Taylor series expansions), which considerably simplified the equations of motion, which in turn led to tractable response and stability calculations.

The present work addresses the large crank, and methods for determining response and stability are presented. Basically, there are two approaches to such tasks; namely, finite element approaches, as was done by Song and Haug [2] and Bahgat and Willmert [3], and mode methods. Generally speaking, mode methods are more efficient, requiring fewer degrees of freedom to be carried in the analysis for an accurate solution. However, they are less general in that they can only readily be used for shapes for which the modes are easily derived. Here, a Galerkin approach and a polynomial mode method are examined. Both of these methods require the use of time dependent mode shapes. Recent publications have examined parametric vibration stability and the response of flexible slider–crank and cam–follower mechanism systems; see, for example, Tadjbakhsh [12], Tadjbakhsh and Yountis [13], Zadoks and Midha [14, 15], Fahrang and Midha [16], Mahyuddin and Midha [17] and Mahyuddin *et al.* [18].

0022–460X/93/210463 + 14 $08.00/0

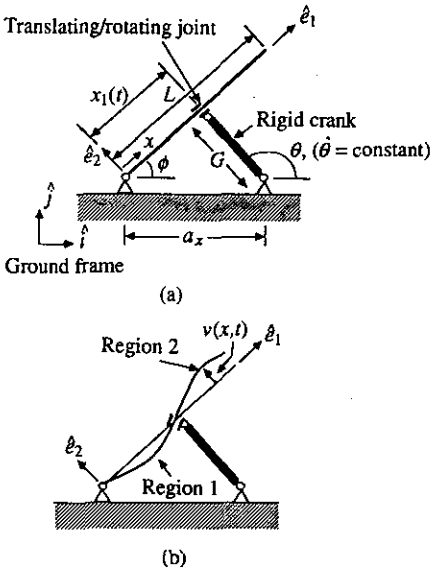

Figure 1. Rigid crank, flexible rod quick return mechanism: (a) Undeformed initial state; (b) deformed state.

The applicability of the free–free mode method to the current problem is also addressed. The technique requires describing the deformation relative to certain co-ordinate frames (such as, for example, a Bucken's frame) and is detailed in reference [4]. The method has several attractive features, namely: (1) the mode shapes are time independent; (2) the technique can be implemented in a rigid body dynamics code (see references [4] and [5]); (3) it leads to sparse matrices.

In all cases, a fourth order Runge–Kutta numerical integration scheme was selected for obtaining the response.

2. RESPONSE

2.1. GALERKIN METHOD

The basic configuration of the system is set forth in Figure 1. The equations of motion for the mechanism were derived in reference [1] and are repeated here for completeness. In non-dimensional form they are

$$\frac{\lambda^2}{\dot{\theta}^2}\frac{\partial^4 w}{\partial \eta^4}+\frac{\partial^2 w}{\partial \theta^2}+\frac{1}{(1+\varepsilon^2+2\varepsilon\cos\theta)^2}[(\eta\varepsilon(\varepsilon^2-1)\sin\theta-w\varepsilon^2(\cos\theta+\varepsilon)^2)]=0,$$

$$0<\eta<\bar{l},\ \bar{l}<\eta<1, \tag{1}$$

where

$$\theta=\dot{\theta}t, \qquad w(\eta,\theta)=v(x,t)/L,$$
$$\varepsilon=G/a_x, \qquad \eta=x/L, \qquad \bar{l}=x_1/L, \qquad \lambda^2=EI/(\bar{m}L^4) \tag{2}$$

and where a_x is the base length. The non-dimensional essential boundary conditions are

$$w(\bar{l},\theta)=0, \qquad \frac{\partial w}{\partial \eta}(\bar{l}^+,\theta)=\frac{\partial w}{\partial \eta}(\bar{l}^-,\theta), \qquad w(0,\theta)=0, \tag{3}$$

and the non-dimensional natural boundary conditions are

$$\frac{\partial^2 w}{\partial \eta^2}(\bar{l}^+, \theta) = \frac{\partial^2 w}{\partial \eta^2}(\bar{l}^-, \theta), \qquad \frac{\partial^2 w}{\partial \eta^2}(0, \theta) = 0, \qquad \frac{\partial^2 w}{\partial \eta^2}(1, \theta) = 0, \qquad \frac{\partial^3 w}{\partial \eta^3}(1, \theta) = 0. \quad (4)$$

In using Galerkin's method, the mode shapes chosen are those for the pinned–pinned beam with an overhang and are time dependent. Denoting them by e_{n1}, $0 < \eta < \bar{l}$, and e_{n2}, $\bar{l} < \eta < 1$, the following trial functions are used:

$$w_{T1}(\eta, \theta) = \sum_{n=1}^{N} f_n(\theta) e_{n1}(\eta, \theta), \qquad 0 < \eta < \bar{l}, \quad (5)$$

$$w_{T2}(\eta, \theta) = \sum_{n=1}^{N} f_n(\theta) e_{n2}(\eta, \theta), \qquad \bar{l} < \eta < 1. \quad (6)$$

Application of Galerkin's method with these trial functions leads to (see reference [1] for more detail):

$$\Delta_{kk} \frac{\mathrm{d}^2 f_k}{\mathrm{d}\theta^2} + \sum_{n=1}^{N} \bar{a}_{kn} \frac{\mathrm{d}f_n}{\mathrm{d}\theta} + f_k \left(\frac{\omega_k^2}{\theta^2} \Delta_{kk} - \frac{\varepsilon^2 (\cos\theta + \varepsilon)^2}{(1 + 2\varepsilon \cos\theta + \varepsilon^2)^2} \Delta_{kk} \right)$$
$$+ \sum_{n=1}^{N} \bar{b}_{kn} f_n = \frac{-\varepsilon \sin\theta (\varepsilon^2 - 1)}{(1 + 2\varepsilon \cos\theta + \varepsilon^2)^2} \bar{g}_k, \qquad k = 1, \ldots, N, \quad (7)$$

where

$$\Delta_{kk} = \int_0^{\bar{l}} e_{k1} e_{k1} \, \mathrm{d}\eta + \int_{\bar{l}}^{1} e_{k2} e_{k2} \, \mathrm{d}\eta, \quad (8)$$

$$\bar{a}_{kn} = 2 \left(\int_0^{\bar{l}} e_{k1} \frac{\partial e_{n1}}{\partial \theta} \, \mathrm{d}\eta + \int_{\bar{l}}^{1} e_{k2} \frac{\partial e_{n2}}{\partial \theta} \, \mathrm{d}\eta \right), \quad (9)$$

$$\bar{b}_{kn} = \int_0^{\bar{l}} e_{k1} \frac{\partial^2 e_{n1}}{\partial \theta^2} \, \mathrm{d}\eta + \int_{\bar{l}}^{1} e_{k2} \frac{\partial^2 e_{n2}}{\partial \theta^2} \, \mathrm{d}\eta, \quad (10)$$

$$\bar{g}_k = \int_0^{\bar{l}} \eta e_{k1} \, \mathrm{d}\eta + \int_{\bar{l}}^{1} \eta e_{k2} \, \mathrm{d}\eta. \quad (11)$$

ω_k is the kth natural frequency of a pinned–pinned beam with an overhang. Analytic expressions for the integrals in equations (7)–(11) were sought using the symbolic manipulator REDUCE [6]. However, they proved so unwieldy that the approach was abandoned. A purely numerical approach was adopted, in which the integrals were evaluated using the quadrature routine NAAS:QCRP [7]. The partial derivatives in the integrands were treated via finite differences, and the ordinary differential equations (7) were integrated using a fourth order Runge–Kutta method.

Some trial calculations were made using a very flexible rod, with the properties: $L = 1$ m, $a_x = 0{\cdot}59997$ m, $b = 0{\cdot}05$ m, $h = 0{\cdot}05$ m, $E = 0{\cdot}7 \times 10^{11}$ N/m^2, $I = 0{\cdot}5208 \times 10^{-6}$ m^4, $\bar{m} = 7{\cdot}15$ kg/m, $G = 0{\cdot}0059997$ m. The tip response for a crank speed of 100 rad/s was determined. One- and two-mode approximations took of the order of 25 minutes and 75 minutes, respectively, on an Apollo 4000 computer. This alone would be acceptable, but

stability also has to be addressed. Using the monodromy matrix method set forth, for example, in Meirovitch [8], it was estimated that each single data point on a stability chart would involve roughly 300 minutes of computation time for a two-mode approximation. In view of this unacceptable time, the approach was abandoned. It should be noted that techniques do exist to speed up the determination of the monodromy matrix [19, 20], but they were not considered because they are approximate.

2.2. POLYNOMIAL MODES

In an effort to find a less computationally intensive technique, a time dependent polynomial mode approach was developed. In variational methods, admissible functions need only satisfy the essential boundary conditions. A simple set of time dependent, linearly independent polynomials satisfying only the essential boundary conditions are given below:

$$\phi_{11}=x(x-x_1), \quad 0<x<x_1; \qquad \phi_{12}=x_1(x-x_1), \quad x_1<x<L; \tag{12}$$

$$\phi_{21}=x^2(x-x_1), \quad 0<x<x_1; \qquad \phi_{22}=x_1x(x-x_1), \quad x_1<x<L; \tag{13}$$

$$\vdots$$

$$\phi_{n1}=x^n(x-x_1), \quad 0<x<x_1; \qquad \phi_{n2}=x_1x^{n-1}(x-x_1), \quad x_1<x<L. \tag{14}$$

Note that these expressions depend on time, through the parameter x_1.

These time dependent polynomials can be applied directly to the Euler–Lagrange equation

$$\frac{\mathrm{d}}{\mathrm{d}t}\frac{\partial \mathscr{L}}{\partial \dot{f}_i}-\frac{\partial \mathscr{L}}{\partial f_i}=0, \tag{15}$$

where the Lagrangian $\mathscr{L}$ is given in terms of the dimensional transverse displacement v and the angle ϕ (see Figure 1) by

$$\begin{aligned}\mathscr{L}=&\frac{\bar{m}}{2}\int_0^{x_1}\left(\left(\left(\frac{\partial v}{\partial t}\right)^2+2x\frac{\partial v}{\partial t}\dot{\phi}+x^2\dot{\phi}^2+v^2\dot{\phi}^2\right)\right)\mathrm{d}x\\&+\frac{\bar{m}}{2}\int_{x_1}^{L}\left(\left(\left(\frac{\partial v}{\partial t}\right)^2+2x\frac{\partial v}{\partial t}\dot{\phi}+x^2\dot{\phi}^2+v^2\dot{\phi}^2\right)\right)\mathrm{d}x\\&-\frac{EI}{2}\int_0^{x_1}\left(\frac{\partial^2 v}{\partial x^2}\right)^2\mathrm{d}x-\frac{EI}{2}\int_{x_1}^{L}\left(\frac{\partial^2 v}{\partial x^2}\right)^2\mathrm{d}x.\end{aligned} \tag{16}$$

Assume for v a trial solution of the form (using the summation convention hereafter)

$$v_{T1}=f_i(t)\phi_{i1}, \quad 0<x<x_1, \qquad v_{T2}=f_i(t)\phi_{i2}, \quad x_1<x<L. \tag{17}$$

Equations (15), (16) and (17) give, after considerable algebra,

$$\bar{m}\Gamma_{1ij}\ddot{f}_j+2\bar{m}\Gamma_{2ij}\dot{f}_j+(\bar{m}\Gamma_{3ij}-\bar{m}\dot{\phi}^2\Gamma_{1ij}+EI\Gamma_{4ij})f_j=-\bar{m}\ddot{\phi}\Gamma_{5i}, \tag{18}$$

where

$$\Gamma_{1ij}=x_1^{i+j+3}\left(\frac{1}{i+j+3}-\frac{2}{i+j+2}+\frac{1}{i+j+3}\right)$$
$$+x_1^2\left(\frac{L^{i+j+1}-x_1^{i+j+1}}{i+j+1}-\frac{2x_1(L^{i+j}-x_1^{i+j})}{i+j}+\frac{x_1^2(L^{i+j-1}-x_1^{i+j-1})}{i+j-1}\right), \tag{19}$$

$$\Gamma_{2ij}=-\dot{x}_1x_1^{i+j+2}\left(\frac{1}{i+j+2}-\frac{1}{i+j+1}\right)$$
$$+\dot{x}_1x_1\left(\frac{L^{i+j+1}-x_1^{i+j+1}}{i+j+1}-\frac{3x_1(L^{i+j}-x_1^{i+j})}{i+j}+\frac{2x_1^2(L^{i+j-1}-x_1^{i+j-1})}{i+j-1}\right), \tag{20}$$

$$\Gamma_{3ij}=-\ddot{x}_1x_1^{i+j+2}\left(\frac{1}{i+j+2}-\frac{1}{i+j+1}\right)+\frac{x_1\ddot{x}_1}{i+j+1}(L^{i+j+1}-x_1^{i+j+1})$$
$$+\frac{-2x_1\dot{x}_1^2-3x_1^2\ddot{x}_1}{i+j}(L^{i+j}-x_1^{i+j})+\frac{2x_1^2\dot{x}_1^2+2x_1^3\ddot{x}_1}{i+j-1}(L^{i+j-1}-x_1^{i+j-1}), \tag{21}$$

$$\Gamma_{411}=4x_1/L^4, \tag{22}$$

$$\Gamma_{41j}=2x_1^j/L^{j+3}, \qquad i=1, \quad j\neq 1, \tag{23}$$

$$\Gamma_{4i1}=2x_1^i/L^{i+3}, \qquad j=1, \quad i\neq 1, \tag{24}$$

$$\Gamma_{422}=(4x_1^3+4x_1^2(L-x_1))/L^6. \tag{25}$$

For all other i and j:

$$\Gamma_{4ij}=ijx_1^{i+j-1}\left(\frac{(i+1)(j+1)}{i+j+1}-\frac{2(ij-1)}{i+j-2}+\frac{(i-1)(j-1)}{i+j-3}\right)+x_1^2(i-1)(j-1)$$
$$\times\left[\frac{ij(L^{i+j-3}-x_1^{i+j-3})}{i+j-3}-\frac{x_1((i-2)j+i(j-2))(L^{i+j-4}-x_1^{i+j-4})}{i+j-4}\right.$$
$$\left.+\frac{x_1^2(i-2)(j-2)(L^{i+j-5}-x_1^{i+j-5})}{i+j-5}\right], \tag{26}$$

$$\Gamma_{5i}=x_1^{i+3}\left(\frac{1}{i+3}-\frac{1}{i+2}\right)+x_1\frac{(L^{i+2}-i+2)}{i+2}-\frac{x_1^2(L^{i+1}-i+1)}{i+2}. \tag{27}$$

To test the procedure, the small crank problem treated in reference [1] was solved, using a Runge-Kutta integration scheme on equations (18). Excellent agreement was found lending confidence to the approach.

To test the polynomial modes on a large crank problem, the properties and dimensions used by Bahgat and Willmert [3] in their finite element study were used, namely, $G=1{\cdot}5$ in, $L=9{\cdot}3746$ in, $a_x=4$ in, $EI=2{\cdot}91992\text{E}6$ lbf in^2, $\bar{m}=0{\cdot}1268$ lbm/in and $\dot{\theta}=90$ rad/s.

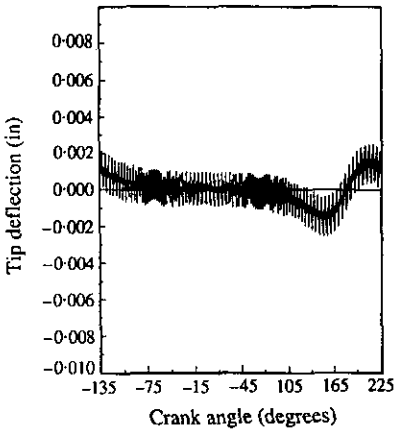

Figure 2. Large crank-tip deflection using three polynomial modes.

Tip deflections using 3 and 10 modes are shown in Figures 2 and 3. Note that most of the deflection is captured by 3 modes. Bahgat and Willmerts' results for the horizontal ($\hat{i}$ in Figure 1) and vertical components ($\hat{j}$ in Figure 1) of the tip deflection, U_3 and V_2, respectively, are shown in Figure 4. Note the absence of high frequency oscillations, such as occur in Figures 2 and 3. When 0·2 percent proportional damping is included, the results displayed in Figure 5 show trends similar to those of Figure 4. This conclusion was made from the observation that Figure 4 deformations constitute a vector that is directed almost perpendicularly to the rod axis at any time; hence the deformation is almost entirely bending deformation (axial deformation was also included in their analysis). An approximation of Figure 4 deformation in the floating frame of Figure 1 is therefore $\sqrt{U_3^2+V_2^2}$, and since U_3 is always small compared to V_2, the deformation is approximately V_2. Hence, Figures 5 and the second plot of Figure 4 can be directly compared, and they do indeed display similar trends. Exact agreement is not to be expected because Bahgat and Willmert included effects not considered in this analysis, i.e., a flexible crank, a flexible sliding link, and axial deformation of all links. Note that the presentation of the crank angle in Figure 5 is phase shifted to account for different mechanism configurations chosen

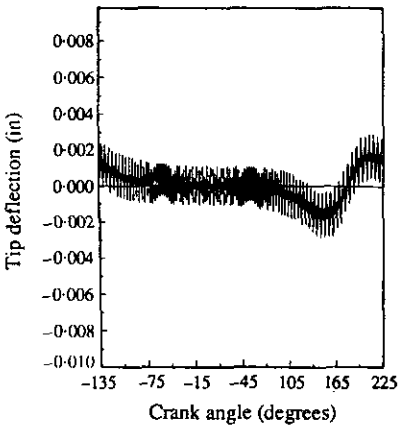

Figure 3. Large crank-tip deflection using ten polynomial modes.

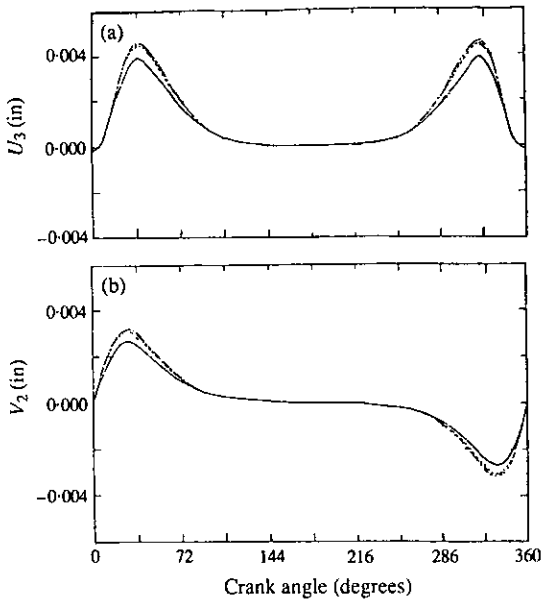

Figure 4. Large crank-tip deflection results from reference [3], 1·5 inch crank: ——, three elements; - - -, five elements; — - —, seven elements. Deformations (a) U_3 and (b) V_2.

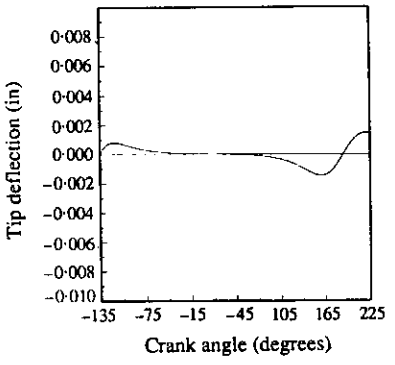

Figure 5. Ten polynomial mode approximation to large crank problem with 0·002 damping.

for the zero angle position. Steady state was immediately achieved in Figure 5 for zero initial position and velocity of the modes.

2.3. FREE FREE MODES

The free–free mode method, which is reasonably well known in the aerospace industry, has recently been applied to more mechanical engineering oriented applications. In references [4] and [5] it was implemented for mechanisms with pinned end constraints. Also, Buffington and Kane [9] applied it to the problem of a flexible magnetic tape moving over a pair of fixed supports.

The free–free modes in question are with respect to a "shadow" or "floating" frame that is moving with the flexible object. The shadow frame and the flexible object are kept close to each other by imposition of a set of constraint relations. Many floating frames

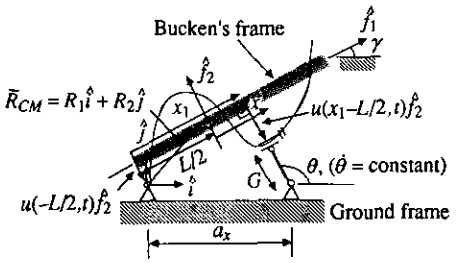

Figure 6. Free-free mode description of quick return mechanism.

are available. The one chosen here is the Bucken's frame, also known as a linearized Tisserand frame [10].

The system is shown in terms of a Bucken's frame in Figure 6. Generalized co-ordinates R_1 and R_2 are the components of a vector from ground to the center of mass of the deformed beam, where the origin of the shadow beam is located. The angle γ, a generalized co-ordinate, between the vector $\hat{f}_1$ in the floating frame and ground, is not prescribed at this stage.

The elastic deformation, now defined as $u(x, t)$, with respect to the floating frame is written

$$u = \sum_{i=1}^{n} f_i(t)\psi_i(x), \tag{28}$$

where f_i is the generalized co-ordinate corresponding to $\psi_i(x)$, which is the ith orthonormalized Euler–Bernoulli mode shape for a free-free beam. (These functions are well known and are not reproduced here.)

The constraint relations Φ_i, which will be specified later, are handled by the introduction of an augmented Lagrangian Λ, defined by

$$\Lambda = T - V + \sum_{j=1}^{m} \lambda_j \Phi_j, \tag{29}$$

where λ_j are Lagrange multipliers. Instead of equation (15), the associated Euler–Lagrange equations are now

$$\frac{\mathrm{d}}{\mathrm{d}t}\left(\frac{\partial \Lambda}{\partial \dot{q}_i}\right) - \frac{\partial \Lambda}{\partial q_i} = 0, \qquad i = 1, \ldots, n, \tag{30}$$

$$\frac{\partial \Lambda}{\partial \lambda_j} = \Phi_j(q, t) = 0, \qquad j = 1, \ldots, m, \tag{31}$$

where the q_i denote the generalized co-ordinates.

The position vector from the ground to any material point on the beam is given by

$$\bar{r} = R_1\hat{i} + R_2\hat{j} + x\hat{f}_1 + u\hat{f}_2. \tag{32}$$

From this, the rod kinetic energy can be obtained as

$$T_{rod} = \bar{m}\int_{-L/2}^{L/2} (\dot{R}_1^2/2 + \dot{R}_2^2/2 - \dot{\gamma}u(\dot{R}_1\cos\gamma + \dot{R}_2\sin\gamma) + \dot{\gamma}x(\dot{R}_2\cos\gamma - \dot{R}_1\sin\gamma) + \dot{u}(\dot{R}_2\cos\gamma - \dot{R}_1\sin\gamma) + (\dot{\gamma}^2/2)(u^2 + x^2) + \dot{\gamma}x\dot{u} + (\dot{u}^2/2)\,\mathrm{d}x. \tag{33}$$

The modes ψ_i have the properties

$$\int_{-L/2}^{L/2} \psi_i \psi_j \, dx = \delta_{ij}, \qquad \int_{-L/2}^{L/2} \psi_i \, dx = 0, \qquad \int_{-L/2}^{L/2} x \psi_i \, dx = 0, \tag{34–36}$$

where δ_{ij} denotes the Kronecker delta. Using these properties, equation (33) becomes

$$T_{rod} = (\bar{m}/2)(L\dot{R}_1^2 + L\dot{R}_2^2 + \dot{\gamma}^2 f_i f_i + \dot{\gamma}^2 L^3/12 + \dot{f}_i \dot{f}_i). \tag{37}$$

The strain energy V is given by

$$V_{rod} = \frac{EI}{2} \int_{-L/2}^{L/2} (\partial^2 u/\partial x^2)^2 \, dx. \tag{38}$$

Using the mode property

$$\int_{-L/2}^{L/2} \frac{d^2\psi_i}{dx^2} \frac{d^2\psi_j}{dx^2} \, dx = k_i^4 \delta_{ij}, \tag{39}$$

equation (38) becomes

$$V_{rod} = (EI/2) k_j^4 f_j^2. \tag{40}$$

The generalized co-ordinates are f_i, R_1, R_2 and γ, but three independent scalar constraint equations exist. The first two come from a vector loop around the pin grounding the flexible rod:

$$\bar{R}_{cm} - (L/2)\hat{f}_1 + u(-L/2, t)\hat{f}_2 = 0. \tag{41}$$

Taking the scalar product of this equation with $\hat{f}_1$, $\hat{f}_2$ yields

$$\Phi_1 \equiv R_1 \cos\gamma + R_2 \sin\gamma - L/2 = 0, \tag{42}$$

$$\Phi_2 \equiv -R_1 \sin\gamma + R_2 \cos\gamma + u(-L/2, t) = 0. \tag{43}$$

A vector loop around the translating joint gives the third constraint equation

$$\bar{R}_{cm} + \left(x_1 - \frac{L}{2}\right)\hat{f}_1 + u\left(x_1 - \frac{L}{2}, t\right)\hat{f}_2 - G(\cos\theta \hat{i} + \sin\theta \hat{j}) - a_x \hat{i} = 0. \tag{44}$$

Taking the scalar product of equation (44) with $\hat{f}_1$ yields an expression for x_1 from which $\dot{x}_1$ can be obtained. Taking the scalar product of equation (44) with $\hat{f}_2$ and substituting the values found for x_1 and $\dot{x}_1$ gives the third constraint equation:

$$\Phi_3 = -R_1 \sin\gamma + R_2 \cos\gamma + u(x_1 - L/2, t) + G \sin(\gamma - \theta) + a_x \sin\gamma = 0. \tag{45}$$

Substituting equations (37), (40), (42), (43), (45) and (28) into equations (30) gives the equations

$$\bar{m}L\ddot{R}_1 - \lambda_1 \cos\gamma + \lambda_2 \sin\gamma + \lambda_3 \sin\gamma = 0, \tag{46}$$

$$\bar{m}L\ddot{R}_2 - \lambda_1 \sin\gamma - \lambda_2 \cos\gamma - \lambda_3 \cos\gamma = 0, \tag{47}$$

$$\begin{aligned} &\bar{m}(L^3/12)\ddot{\gamma} + \bar{m} f_i f_i \ddot{\gamma} + 2\bar{m}\dot{\gamma} f_i \dot{f}_i + \lambda_1 R_1 \sin\gamma - \lambda_1 R_2 \cos\gamma + \lambda_2 R_1 \cos\gamma \\ &\quad + \lambda_2 R_2 \sin\gamma + \lambda_3 R_1 \cos\gamma + \gamma_3 R_2 \sin\gamma - \lambda_3 G \cos(\gamma - \theta) \\ &\quad - \lambda_3 a_x \cos\gamma + \lambda_3 f_i \frac{d\psi_i}{dx}(@x_1 - L/2)(a_x \sin\gamma + G \sin(\gamma - \theta)) = 0, \end{aligned} \tag{48}$$

$$\bar{m}\ddot{f}_i - \bar{m}\dot{\gamma}^2 f_i + EIf_i k_i^4 - \lambda_2 \psi_i(@ - L/2) - \lambda_3 \psi_i(@x_i - L/2) = 0 \qquad \text{(no sum on } i\text{)}. \tag{49}$$

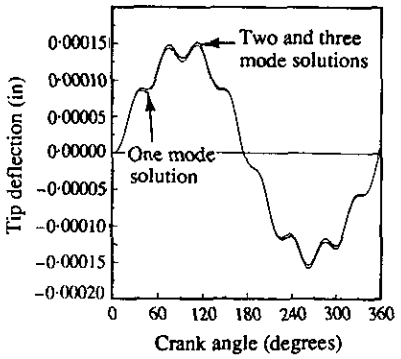

Figure 7. Small crank-tip deflection using one, two and three free–free modes.

A fourth order Runge–Kutta scheme was chosen for the numerical integration. It required that the constraint equations (42), (43) and (45) be differentiated twice, and the use of first order forms. However, the details will not be reproduced here. The initial conditions used were an undeformed beam ($f_i(0)=0$) and $\dot{f}_i(0)=0$. Hence the initial origin of the Bucken's Frame is at the center of mass of the "rigid body", and its initial orientation is defined by $\hat{f}_1$ being along the rigid body axis. The initial geometry and the rigid body kinematics give R_1, R_2, γ and their time derivatives at $t=0$.

For validation purposes, the small crank problem previously treated is first considered. Tip deflection using 1, 2 and 3 modes is shown in Figure 7. Comparing with previous results, a one mode approximation is very accurate and, beyond two modes, no significant increase in accuracy occurs with the addition of more modes.

The stiffer rod used in conjunction with the polynomial mode method was also examined. The tip deflection using 1, 3 and 5 free–free modes is shown in Figures 8–10. Rapid convergence is seen. Note that the results agree quite well with those using the polynomial modes.

Thus it can be concluded that the free–free mode method can successfully and efficiently capture the response of a mechanism in which there is a moving boundary. In the authors' experience, it is actually less costly than the polynomial mode method even though the equations are non-linear. One word of caution, though—in a run in which an instability

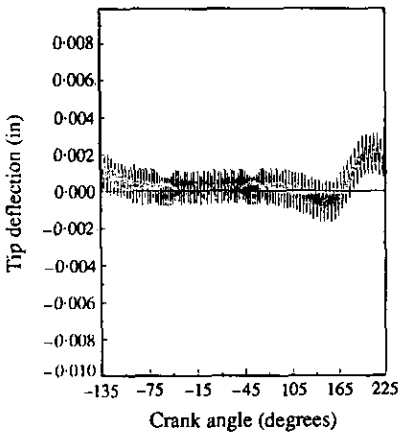

Figure 8. Large crank-tip deflection using one free–free mode.

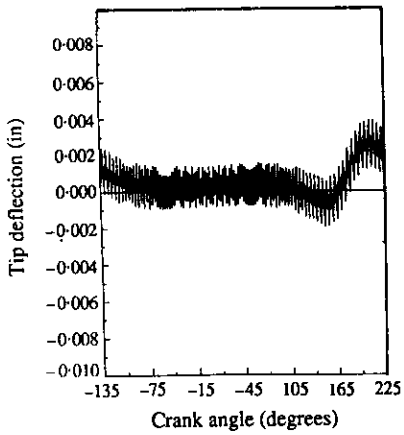

Figure 9. Large crank-tip deflection using three free–free modes.

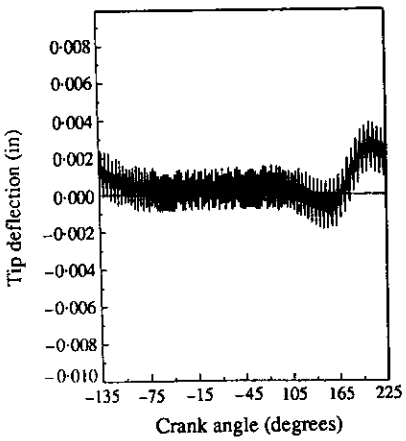

Figure 10. Large crank-tip deflection using five free–free modes.

occurred, so that the deflections became quite large, it was found that the free–free mode method diverged. It is recommended for use for this class of problem only when the deformations are small.

3. STABILITY

3.1. HOMOGENEOUS EQUATION STABILITY

In reference [1] it was shown that homogeneous equation instability zones in $\dot{\theta} - \varepsilon$ plane emanate from the line $\varepsilon = 0$ at points $\dot{\theta} = 2\omega_1/n$, $\dot{\theta} = (\omega_1 + \omega_2)/n$ and $\dot{\theta} = 2\omega_2/n$, $n = 1, 2, 3$, where ω_k is the kth pinned–pinned overhanging beam natural frequency when the crank has zero length. These zones or at least the lower order ones—were obtained using perturbation methods and were confirmed using the monodromy matrix method. Perturbation techniques cannot be employed in the current problem, since ε is not necessarily small. The monodromy matrix method has to be used.

The response has been obtained using both polynomial and free–free modes. The use of the former will be addressed first. As was noted previously, three modes were sufficient to capture the response accurately, and those are all that are considered here (comparisons

with some of the independently obtained small ε stability zones showed that, indeed, retention of just three modes was adequate).

Equations (18) are linear differential equations with time dependent coefficients. Because of the linearity, the monodromy matrix technique can be applied directly. It requires the numerical integration over the crank period of the set of governing differential equations for different sets of initial conditions. This generates a matrix (monodromy matrix) the eigenvalues of which must be determined (their nature determines stability/instability). This procedure must be run through for each $(\dot{\theta}, \varepsilon)$ point and so it is computationally very intensive. However, it is not restricted to small ε values.

The computational strategy was as follows. Potential instability zones emanate from the $\dot{\theta}$-axis where $\varepsilon = 0$. To determine these points, consistent with the three-mode approximation, ε was set equal to zero in equation (18) and the resulting eigenvalue problem solved numerically. Rather than go through the very computationally intensive effort of generating a stability chart, it was decided instead just to search for instabilities in the range of practical speeds and sizes, which was taken to be as follows: $\dot{\theta}$ between 0 and 20 rad/s and ε such that $\varepsilon \leqslant 0{\cdot}3$. Using the properties specified previously for the very flexible rod, the monodromy matrix method did not reveal any instabilities in the practical range. Thus, for the stiffer configuration likely to be encountered in practice, it can be concluded even more strongly that homogeneous equation instabilities do not occur for practical operating speeds.

Problems arise in addressing instabilities using the free–free mode method. The free–free equations (46)–(49) are non-linear, and so would have to be linearized before stability could be addressed. A possible approach to such a linearization is one in which the co-ordinate γ (see Figure 6) would be replaced by an angle measure from the $\hat{f}_1$ axis. It is conjectured that a small angle approximation would then lead to a set of linearized equations to which standard methods could be applied. Buffington and Kane [9] used a similar technique for their problem and it led to a set of linear equations for stability analysis. However, the approach suffers from the shortcoming that such co-ordinates are not ones used in commercial codes, such as ADAMS [11]. Procedures to generalize the process of linearization so as to be applicable to a set of generalized co-ordinates defined with respect to ground are not obvious, and the issue is left as an open question. In view of these problems, the possible use of free–free modes for addressing stability is left for future work.

3.2. INHOMOGENEOUS EQUATION STABILITY

In reference [1] it was shown that in the small crank problem there were instabilities due to the inhomogeneous terms in equations (7). They arose at crank speeds equal to $1/n$ times the first natural frequency of the overhanging beam for zero crank length ($\varepsilon = 0$). For non-zero ε, there is no fixed natural frequency of the overhanging beam, since the location of the pivot point changes appreciably during a cycle. In Figure 11, for example, variation of the first natural frequency with the crank angle (and hence the pivot location) is shown for $\varepsilon = 0{\cdot}2$. Large variations are seen. Under these circumstances, it is not clear whether or not the instabilities found in reference [1] occur.

Using numerical integration of equations (18), the tip deflection, using three polynomial modes and the flexible beam configuration, was obtained at a crank speed equal to the average natural frequency (=900 rad/s) for $\varepsilon = 0{\cdot}2$. The result is shown in Figure 12. A beating, but not unbounded, motion is seen. However, for all practical purposes the motions can be regarded as unstable, since the amplitudes involved are so large (of the order of meters!). Thus, in this sense, the instabilities are still present. As in reference [1], though, they are at speeds well outside the practical range.

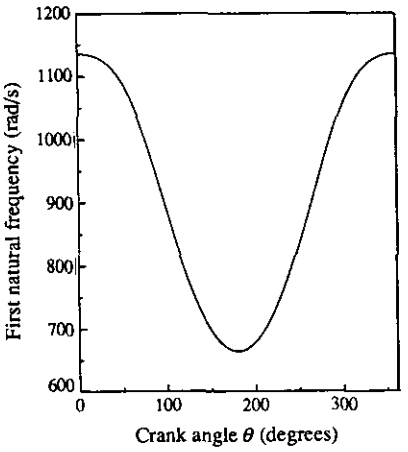

Figure 11. First natural frequency using three polynomial modes, versus crank angle, at $\varepsilon = 0{\cdot}2$.

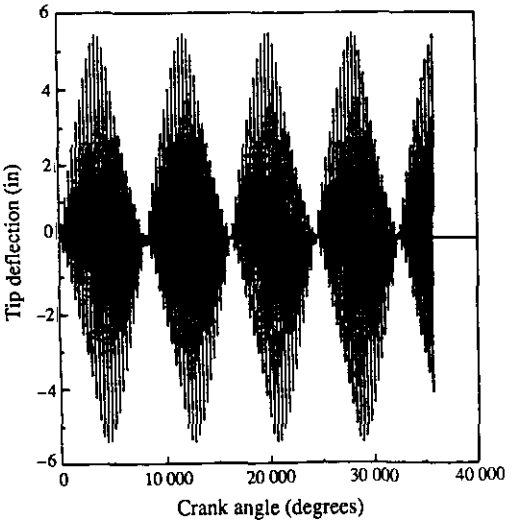

Figure 12. Tip deflection at $\dot{\theta}$ = average first natural frequency, $\varepsilon = 0{\cdot}2$.

Numerical integrations were also carried out for crank speeds equal to 1/10 times the averaged first natural frequencies for $\varepsilon = 0{\cdot}1$, $0{\cdot}05$, $0{\cdot}10$ and $0{\cdot}20$. The peak values of the tip displacement were all found to be small, with no discernible instabilities arising.

Thus, in summary it can be concluded that, as in the small crank case, instabilities due to the inhomogeneous terms in the equations of motion arise, but they are at crank speeds well above any anticipated practical speeds.

4. CONCLUSIONS

Three mode methods (Galerkin, polynomial and free–free) have been presented as means of investigating the stability and response when the crank is large. Of the three, the Galerkin method (using time dependent modes) was accurate but too computationally intensive for stability investigations. The polynomial mode method also required time dependent modes and captured most of the tip deflection with three modes. The polynomial mode method was efficient enough to be useful for studying stability by the computational

monodromy matrix method. No parametric resonance instabilities were found at crank speeds in the practical range. The free–free mode method, which employed time independent mode shapes and the Bucken's frame, was shown to capture the response of a mechanism in which there is a moving boundary. The free–free mode method was the most computationally efficient method for response, even though constraint equations were required. However, the equations were non-linear, and stability using those equations is an open question. Lastly, the inhomogeneous equation instability did not occur during the practical range of crank speeds.

REFERENCES

1. D. G. BEALE and R. A. SCOTT 1990 *Journal of Sound and Vibration* **141**, 277–289. The stability and response of a flexible rod in a quick return mechanism.
2. J. O. SONG and E. J. HAUG 1980 *Computer Methods in Applied Mechanics and Engineering* **24**, 359–381. Dynamic analysis of planar mechanisms.
3. B. M. BAHGAT and K. D. WILLMERT 1976 *Mechanisms and Machine Theory* **11**, 47–71. Finite element vibrational analysis of planar mechanisms.
4. T. J. WIELENGA 1984 *Ph.D. Dissertation, University of Michigan*. Simplification in the simulation of mechanisms containing flexible members.
5. W. J. YOO and E. J. HAUG 1986 *Journal of Mechanisms, Transmissions and Automation in Design* **108**, 315–322. Dynamics of flexible mechanical systems using vibration and static correction modes.
6. L. R. SEWARD 1985 *Reduced User's Guide for IBM* 360 *and Derivative Computers, Version* 3.2. Santa Monica: The Rand Corporation.
7. L. HARDING 1979 *Numerical Analysis and Application Software Abstracts, Computer Center Memo* 407. Ann Arbor, Michigan: The University of Michigan.
8. L. MEIROVITCH 1975 *Method of Analytical Dynamics*. New York: McGraw-Hill.
9. K. W. BUFFINGTON and T. R. KANE 1985 *International Journal of Solids and Structures* **21**, 617–643. Dynamics of a beam moving over supports.
10. J. R. CANAVIN and P. W. LIKINS 1977 *Journal of Spacecraft* **14**, 724–731. Floating reference frames for flexible spacecraft.
11. *ADAMS User's Manual, Version* 5.2, 1987. Ann Arbor, Michigan: Mechanical Dynamics Inc.
12. I. G. TADJBAKHSH 1982 *Journal of Mechanical Design* **104**, 698–703. Stability of motion of elastic planar linkages with application to slider–crank mechanism.
13. I. G. TADJBAKHSH and C. J. YOUNTIS 1986 *Journal of Mechanisms, Transmissions, and Automation in Design* **108**, 487–496. Dynamic stability of the flexible connecting rod of a slider crank mechanism.
14. R. I. ZADOKS and A. MIDHA 1987 *Journal of Mechanism, Transmissions, and Automation in Design* **109**, 210–215. Parametric stability of a two-degree-of-freedom machine system, part I equations of motion and stability.
15. R. I. ZADOKS and A. MIDHA 1987 *Journal of Mechanisms, Transmissions, and Automation in Design* **109**, 216–223. Parametric stability of a two-degree-of-freedom machine system, part II stability analysis.
16. K. FARHANG and A. MIDHA 1989 *Proceedings of the* 1*st National Applied Mechanisms and Robotics Conference, Cincinnati, Ohio*, 3B-7-1–3B-7-7. A model for studying parametric stability in slider–crank mechanisms with flexible coupler.
17. A. I. MAHYUDDIN and A. MIDHA 1990 *Proceedings of the* 21*st Biennial ASME Mechanism Conference, Chicago*, **26**, 11–21. Influence of varying cam profile and follower motion event types on parametric stability.
18. A. I. MAHYUDDIN, A. MIDHA and A. K. BAJAJ 1990 *Proceedings of the* 21*st Biennial ASME Mechanism Conference, Chicago, Illinois* **26**, 1–9. On methods of evaluation of parametric stability and response of flexible cam follower systems.
19. P. FRIEDMANN, C. E. HAMMOND and T. H. WOO 1977 *International Journal of Numerical Methods in Engineering* **11**, 1117–1136. Efficient numerical treatment of periodic systems with application to the stability problems.
20. C. S. HSU 1974 *Journal of Mathematical Analysis and Applications* **45**, 234–251. On approximating a general linear periodic system.